Copper nanoparticles – a promising additive for lubrication of hydrogen technology

[1)] *Monica Ratoi, [2)] Hiroyoshi Tanaka, [1)] Grigore Cernalevschi, [2)]Joichi Sugimura

1) Faculty of Engineering and Physical Sciences, Department of Mechanical Engineering, University of Southampton, Highfield Campus, Southampton, SO17 1BJ, United Kingdom

2) Research Centre for Hydrogen Industrial use and Storage, Kyushu University, 744 Motooka, Nishi-ku, Fukuoka 819-0395, Japan

* Corresponding author email: m.ratoi@soton.ac.uk

Abstract

Bearings used in hydrogen technology face significant lubrication challenges. The main difficulty stems from hydrogen molecules dissociating into atoms on the nascent wear sites and diffusing into steel, ultimately causing hydrogen embrittlement and failure of tribological components. Lubricant additives that rapidly form tribofilms such as antiwear and extreme pressure additives can suppress atomic hydrogen generation and permeation in steel, but the resulting tribofilms tend to increase friction. Nanol™, a sustainable copper-based nanoadditive capable of forming stable dispersions in oils, offers unique friction modifying, antiwear and thermal advantages. In this study, Nanol™ dispersed in a polyalphaolefin base oil was used to lubricate ball and roller bearings undergoing rolling contact fatigue tests under boundary lubrication conditions in a hydrogen environment. Beyond its ability to reduce friction by immediately decreasing the real contact area between the moving parts, Nanol™ also reacts with nascent iron to form cohesive, low friction tribofilms composed of copper and iron oleate on the wear track. These mechanisms, along with the properties of the chemically formed tribofilm were key to lowering friction and extend the fatigue life of the bearings operating in hydrogen and under severe conditions.

Introduction

The use of hydrogen as a fuel is one of the most promising strategies for reducing carbon emissions. Nonetheless, hydrogen technology introduces new challenges for lubricated tribological components (such as rolling element bearings and valves). In addition to operating under high contact pressures, these components must also resist hydrogen embrittlement (HE). Freshly generated wear sites on steel surfaces can act as catalytic sites that dissociate environmental hydrogen molecules, hydrocarbon lubricants, and solubilized water. The released atomic hydrogen due to its small size, readily diffuses into the steel leading to HE [1]-[8].

Studies investigating the influence of hydrogen atmosphere on the rolling contact fatigue (RCF) life of bearings have highlighted the critical role of the tribofilm formed by the lubricant on the wear track in mitigating HE. The tribofilm provides several key functions, the most important of which are: 1) controlling wear and preventing the formation of nascent metal sites that catalyse the decomposition of oil, water and hydrogen molecules and thereby promote atomic hydrogen generation, and 2) acting as a physical barrier that limits hydrogen permeation into the steel.

In a hydrogen atmosphere, tribofilms on wear track may be produced by lubricant additives such as antiwear agents, extreme pressure (EP) additives, and friction modifiers [9], [10] or, in the absence of additives, by the base oil itself [11], [12]. In hydrogen environments, hydrocarbon base oils can form tribofilms through hydrogenolysis, which effectively control wear and reduce hydrogen permeation into bearing steel. These tribofilms typically consist of solidified carbon (from cracking or oxy-polymerization) and iron species in both oxide and elemental forms [11], and their ability to limit hydrogen ingress, mitigate HE, and extend RCF life has been demonstrated. Among additives, ZDDP is one of the most extensively studied antiwear agents. It produces thick tribofilms that significantly decrease hydrogen permeation into steel and improve bearing fatigue life of [10]. WS_2 nanoparticles have similarly been shown to form chemical antiwear tribofilms while also providing the added advantage of reducing friction under boundary regime [9].

These preliminary findings have intensified the search for additives capable of preventing wear and premature bearing failure by forming tribofilms that provide antiwear protection and low friction

In this context, copper and copper-based additives have emerged as promising candidates. As the eighth most abundant major industrial metal on Earth [13], copper is readily available and cost effective. Its full recyclability and resistance to corrosion further make it an environmentally friendly and sustainable option.

Commercial copper oleate is a commonly used oil-soluble friction modifier, valued for its ability to reduce friction and wear through the formation of thick boundary tribofilms. Under certain operating conditions, the additive reacts with nascent iron on the wear track, generating a copper layer and iron oleate, both of which contribute to friction reduction [14].

As a soft metal, copper can also function as a solid lubricant when incorporated as powders or granules in composite materials paired with harder counterparts such as steel, cast iron and aluminium alloys [15]. The resulting antiwear, low friction tribofilms and localized self-repairing protective layers arise from

copper's face centred cubic (FCC) crystal structure and low shear strength, which impart high ductility and toughness [16].

Copper NPs are likewise a promising additive. Owing to their nanoscale size and large surface area, copper NPs exhibit enhanced mechanical properties, including increased strength and hardness. When dispersed in lubricants, they reduce the real contact area between the moving components, which is a key mechanism for minimizing friction and wear under boundary and mixed lubrication regimes typical of NP based additives [17].

Previously published research showed that in sliding applications, copper-based NPs used as lubricant additives in lubricants can reduce wear by 20-48% and friction by 14-35% [17]-[22].

For effective use as lubricant additives, NP surfaces must be functionalised to prevent agglomeration and sedimentation, which could otherwise lead to issues such as filter blockage and abrasive wear caused by large aggregates. Although a range of functionalization agents has been investigated, oleic acid and oleates are generally preferred for tribological applications. Their advantage lies in the ability of the oleate moiety to sterically stabilize NPs in hydrocarbon media, while also adsorbing onto or reacting with metal wear track to form either monolayers resilient to rubbing [23] or reaction products [14], both of which contribute to friction reduction.

Beyond their tribological benefits, functionalized copper NPs can impart excellent thermal and electrical properties to lubricants [24]. As a more cost-effective alternative to silver and gold, non-oxidized copper NPs (produced *in situ* and subsequently functionalized) exhibit exceptionally high thermal and electric conductivities [24], [25]. The thermal conductivity of lubricants containing copper NPs was shown to increase by 31.4% at 70°C when added to automotive gear oils, enhancing heat dissipation and thereby mitigating the reduction in viscosity and film thickness at elevated temperatures. Consequently, the lower CoF achieved by copper NPs additives arises from the combined effects of improved heat conduction and the formation of shear-reducing tribofilms [26].

The combined ability of functionalized copper NPs to reduce friction and wear, dissipate frictional heat, and preserve lubricant properties makes them promising candidate for lubrication of hydrogen technologies. In this study, Nanol™, a commercial additive consisting of copper NPs with sizes ranging from 5 to 30 nm (particle size distribution ~20 nm), functionalized with oleic acid/oleate, and widely applied in automotive, marine, industrial, and power sectors to reduce friction, wear and extend service life was selected.

Materials and methods

A concentration of 1 wt.% Nanol™ additive, as recommend by the manufacturer, was dispersed in synthetic polyalphaolefins PAO32 (Idemitsu Kosan Co. Ltd., Japan; **Table 1**). PAO32 was selected based on previous RCF studies demonstrating its superior overall performance compared to other types of oils of similar viscosity [12]. In both air (oxygen) and hydrogen environments, PAO32 formed tribofilms on the wear tracks composed of iron oxide (as hematite when tested in air) covered by thick carbon layers in the form of micro/nanocrystalline and amorphous graphite. Such tribofilm formation was not observed in inert gases like argon.

The high thermal diffusivity of PAO32 [27], defined as thermal conductivity divided by density and specific heat capacity, helps prevent overheating by facilitating heat dissipation. Combined with its high chemical stability (resistance to thermal and oxidative degradation), this property minimizes the release of atomic hydrogen from the oil. Additionally, the non-polar structure of PAOs reduces water solubility, which is itself a significant source of atomic hydrogen [11].

Rolling contact fatigue (RCF) tests were performed using the tribometer shown in **Fig. 1** with two setups: ball-on-disc (BoD) and roller-on-disc (RoD). A normal load of 2650 N was applied via a lever, corresponding to a Hertzian pressure of 3.3 GPa for ball-disc interface and 1.5 GPa for the roller-disc interface. The disc and rolling element contact underwent rolling motion through rotation of the upper shaft. This contact pressure is below the elastic limit but exceeds typical operating pressures in bearings, and was adopted based on recommendations from previous studies [1]-[3], [28]-[30].

Both setups operated under severe boundary lubrication conditions (lambda parameter of ~0.1) to accelerate wear, promote atomic hydrogen formation, and induce failure through embrittlement.

The ball-on-disc (BoD) setup used commercial thrust ball bearings with a polymer cage, modified so that the grooved top ring served as a guide for the ball movement, while the lower ring was inverted to present its flat surface to the balls. Eighteen balls (6.35 mm diameter) separated by a retainer were used per bearing.

The alternative roller-on-disc setup employed bearings with only three rollers (5 mm diameter) positioned at 120 degrees intervals (**Fig. 2**).

The ball, roller and disc steel was JIS SUJ2, equivalent to AISI 52100. The disc surface was used as received, with a root mean square roughness (R_q) of approximately 0.105 μm. This roughness is considerably higher than in previous studies, where the discs were polished to an R_q of 5 nm [11], and

was chosen to better investigate the friction modifying and antiwear effects of Nanol™. Prior to the testing, all specimens were ultrasonically cleaned in hexane and acetone.

While the BoD contact in bearings involves mostly pure rolling, the RoD bearing experiences a constant 3-10% sliding-rolling ratio (SRR) due to geometrical constraints and the "Heathcote slip" phenomenon. "Heathcote slip" specifies that the contact between the cylindrical thrust bearing and the disc undergoes pure rolling only at the middle of the roller, with slippage increasing linearly toward the roller ends, being positive (in the direction of rolling) at the outer side of the roller and negative at the inner side [31]. The RoD setup in this study was therefore employed to evaluate Nanol™'s ability to mitigate sliding, particularly the negative slippage at the inner side of the roller, which is known to cause severe wear and white etching cracks (WECs) [32].

The RCF lives were determined by the number of rotation cycles completed before the test automatically stopped. The test halted when the vibration amplitudes detected by a sensor on the loading lever exceeded a preset threshold, corresponding to the onset of the first flaking event.

The RCF test conditions are summarized in **Table 1**.

Table 1. RCF test conditions for ball-on-disc and roller-on-disc contacts

Contact geometry	Ball-on-disc (BoD)	Roller-on-disc (RoD)
Bearing type	51107	K81107T2
Test gas	H_2 (99.997% pure)	
Temperature	120ºC	
Base oil PAO32	0.826 g·cm^{-3}, 28.8 mm^2·s^{-1} (40ºC), 5.6 mm^2·s^{-1} (100ºC)	
Nanoadditive	Nanol™ 1 wt.%	
Specimens	JIS SUJ2 steel balls ($R_q \approx 0.005$ µm) / discs ($R_q \approx 0.2$ µm)	JIS SUJ2 steel rollers ($R_q \approx 0.005$ µm)/ discs ($R_q \approx 0.2$ µm)
Number of rolling elements in thrust bearing	18 balls	3 rollers
Hertzian contact	Point	Line
Maximum Hertzian pressure	3.3 GPa	1.5 GPa

Entrainment speed	1500 rpm (3.4 m/s)	
Film parameter Λ	0.11	0.135

The RCF tests were conducted using commercial bearings, and no data on the CoF within the tribological contact were provided. To obtain comparative friction information for the two lubricants (PAO and PAO+Nanol™), tribological tests were performed in an MTM (PCS Instruments) in air, under conditions otherwise similar to those at the interface between the disc and the inner side of the roller, which experiences the largest negative slippage (-10%) (**Table 2**).

Table 2. MTM test conditions for ball-on-disc contact	
Contact geometry	Ball-on-disc (BoD)
Specimens	AISI 52100 19 mm balls & discs R_q =11±3 nm
Test gas	Air
Temperature ºC	120
Load (N)	50
Entrainment speed (mm/s)	40
SRR %	-10
Running time (h)	6
Lambda value	0.135

Thermal desorption spectroscopy (TDS) using a Denshi-Kagaku TDS1200 system was employed to measure the hydrogen content in the bearing steel specimens (balls and discs). Immediately after the rolling contact tests, the disc and ball specimens were cooled to ambient temperature, cleaned with hexane and acetone in an ultrasonic bath, and the disc cut into small pieces (7 x 3.5 x 1 mm, weighing approximately 0.2 g each). During TDS analysis, the disc pieces and balls were heated from ambient temperature to 800 ºC at rates of 60 ºC/min and 10 ºC/min, respectively. The slower heating rate for the balls accounts for their larger mass and thermal inertia. All gaseous species released during heating were analysed using a quadrupole mass spectrometer to quantify hydrogen species.

Wear tracks were initially examined with an Olympus BX41M-LED optical microscope to assess surface wear, deposits, and corrosion. The depth and morphology of the disc wear tracks were then measured using optical profilometry (Bruker ContourGT) which generates a 3D surface profile of the wear track.

Multiple surface profiles were collected for each disc and the average depth values were calculated using the instrument software.

Raman Spectroscopy was employed to examine the tribofilms formed both inside and outside of wear tracks after RCF testing. Measurements were carried out using a ThermoFisher Scientific DXR Raman Microscope with a 455 nm laser and 0.5 mW output power. The laser was focused onto the sample through either a 10x or 100x objective, resulting in spot diameters of 10 or 1 μm, respectively. Acquisition times were adjusted according to the intensity of the Raman signals and continued until a satisfactory signal-to-noise ratio was achieved.

Elemental composition and mapping on the wear track were investigated using a JEOL JAMP 9500 F Auger electron spectrometer with a 10 keV electron beam. Prior to analysis, ion sputtering was performed for 15-60 seconds to remove the surface contamination layer.

To investigate subsurface microstructural alterations and the presence of WECs, the rollers were mounted in Bakelite, ground using 120, 800, 1200 and 4000 grit grinding sheets, followed by polishing with 3 μm, 1 μm and 0.25 μm polishing cloths. The mounted samples were then etched with 2 % Nital (2 vol.% nitric acid in ethanol) and examined for microstructural alterations by optical microscopy and SEM/EDX (JSM-7200F Schottky Field Emission SEM).

Results and Discussion

RCF life and Hydrogen content

RCF tests were performed under boundary lubrication conditions until bearing failure. Multiple tests were conducted with each lubricant (three in the BoD setup and five in the RoD), using either PAO oil or PAO with Nanol™.

Table 3 summarises the BoD test results, including the fatigue life of each test, the components where failure occurred, and the total hydrogen released from the disc and ball specimens during TDS analysis. The measured hydrogen includes all hydrogen containing species, including water [9]. Comparisons between the two lubricants are illustrated in **Fig. 3** (Fatigue life), **Fig. 4** (Weibull plot of fatigue probability versus fatigue life), and **Fig. 5** (Hydrogen content in specimens).

In the BoD setup, the average fatigue life with Nanol™ lubrication was twice that of PAO, increasing from 68 hours to 136 hours. Failures generally occurred due to flaking on the ball, except in one test (BoD_N1) where both the ball and disc experienced flaking.

In both PAO and Nanol™lubricated tests, the balls contained higher hydrogen levels than the discs, which largely contributed to the flaking observed on the balls. However, no direct correlation was found between hydrogen concentration in the specimens and the extended fatigue life observed in the Nanol™ tests.

Table 3. Hydrogen content, fatigue life, and cause of failure in ball bearings (ball-on-disc setup)

Test	Lube	Content of Hydrogen / ppm		Fatigue life x10^4 Cycles	Failure
		Disc	Ball		
BoD_O1	PAO	0.458	0.607	3632.2	Ball
BoD_O2	PAO	0.532	0.762	5334.6	Ball
BoD_O3	PAO	0.418	0.532	5875.2	Ball
BoD_N1	PAO + 1 wt.% Nanol™	0.484	0.574	6862.2	Disc & Ball
BoD_N2	PAO + 1 wt.% Nanol™	0.496	0.872	10362.2	Ball
BoD_N3	PAO + 1 wt.% Nanol™	0.49	0.63	123 12	Ball

As **Table 4**, **Fig. 6** and **Fig. 7** show, the RCF life for the RoD tests which involve considerable sliding between the ends of the roller and disc are shorter than in the BoD tests. With this setup, the fatigue life results are scattered, and the averages for PAO (16.3 hrs) and Nanol™ (19 hrs) along with the comparative Weibull plots do not show a significant improvement with Nanol™. Like the BoD tests, failure occurred from flaking damage on the roller, except for the RoD_O1 test which stopped because of high vibration.

Table 4. RCF life and cause of failure in roller bearings (roller-on-disc setup)

Test	Lube	Fatigue Life / hours	Failure
RoD_O1	PAO	7.43	Vibration
RoD_O2	PAO	14.77	Rolle r
RoD_O3	PAO	15.3	Roller
RoD_O4	PAO	16.2	Roller
RoD_O5	PAO	27.68	Roller

RoD_N1	PAO + 1 wt.% Nanol™	51.33	Roller
RoD_N2	PAO + 1 wt.% Nanol™	12.2	Roller
RoD_N3	PAO + 1 wt.% Nanol™	5.05	Roller
RoD_N4	PAO + 1 wt.% Nanol™	9.52	Roller
RoD_N5	PAO + 1 wt.% Nanol™	16.95	Roller

RCF wear tracks surface and subsurface analysis

The disc and ball/roller wear tracks were initially examined for wear, failure-related damage, and the presence of tribofilm using optical microscopy and optical profilometry.

In the BoD tests, the disc wear tracks were almost uniformly covered by tribofilms (**Fig. 8**), regardless of whether PAO or Nanol™ was used, and the profiles across the wear tracks (**Fig. 9**) revealed no significant differences in wear.

A similar observation was made for the RoD test discs, where all wear tracks were covered by dark streaks with no discernible difference between the PAO and Nanol™ lubricated tracks (**Fig. 10**). The wear track widths (**Fig. 11**) were approximately 5 mm for both PAO (RoD_O2), and Nanol™ (RoD_N2). However, **Fig. 11** also shows that for both lubricants (PAO and Nanol^{TM}), deep wear grooves formed on the inner side of the disc wear tracks due to the rollers' negative sliding.

On the rollers, the only observed damage was localized flaking (**Fig. 10**), which in most cases led to test failure. This flaking occurred on the inner side of the rollers (except for RoD_O3 where it was located at the centre), consistent with the Heathcote phenomenon, where the inner side of roller experiences the largest negative slippage [31]. The outside side, which undergoes positive slippage, remained undamaged.

A marked difference between PAO and Nanol™ lubricated rollers was immediately apparent. PAO rollers were largely covered by dark streaks, whereas Nanol™ rollers, while showing some streaks, were predominantly coated with a smooth, shiny copper-coloured film and exhibited a much smoother, scratch free surface compared to PAO rollers. **Figure 12** shows the surfaces of RoD_N1 and RoD_N2 rollers under dark field and bright field illumination. Bright field imaging exquisitely highlights the smoothness of the Nanol™ tribofilm and the absence of scratches.

Since no significant differences were observed in wear scar dimensions, wear mechanism, or hydrogen concentration in the specimens, the markedly different tribofilms generated by PAO and Nanol™ are likely responsible for the differences in RCF life.

Raman analysis of the disc tribofilms from PAO (BoD_O1, **Fig. 13**) and Nanol™ (BoD_N1, **Fig. 14**) revealed substantial chemical differences. PAO tribofilms consist primarily of magnetite (Fe_3O_4, Raman shifts 678 cm^{-1}), whereas Nanol™ tribofilms have a complex composition, including inorganic compounds such as Cu_2O, CuO (540 and 647 cm^{-1}), magnetite (677 cm^{-1}), inorganic carbons (G and D peaks at 1580 and 1320 cm^{-1}) and organic compounds. Spectra taken outside the Nanol™ wear track also show peaks for Cu_2O, CuO (540 and 647 cm^{-1}), as well as organic and inorganic carbons (1614 and 2861 cm^{-1}) [33]. Similarly, the Raman spectra of the RoD disc wear tracks (**Fig. 15** and **Fig. 16**) show that the PAO lubricated track exhibits peaks corresponding to Fe_3O_4 (675 cm^{-1}) and microcrystalline graphite (1580 cm^{-1}) [34], while the Nanol™ tribofilm displays peaks associated with CuO and Cu_2O (644, 298, 516 cm^{-1}).

The effect of Nanol™ on CoF

To evaluate the effect of the nanoadditive on friction, MTM tests were conducted in air using PAO and PAO containing 1 wt.% Nanol™, under tribological conditions similar to those at the inner side of the roller in the RoD fatigue tests, where the largest negative slippage occurs (-10%). Over a six-hour test period (**Fig. 17**), the friction for PAO+Nanol™ remained relatively constant and was six times lower (average CoF~0.004) than that of PAO alone (average CoF~0.025).

Mechanism of action of Nanol™

To further investigate the composition of tribofilms generated on disc wear tracks by Nanol™ and PAO, Auger analysis (**Fig. 18**) was performed following initial Argon ion etching to remove the contaminated surface layer. Auger mapping of the PAO lubricated RoD_O1 wear track showed a uniform coverage of iron oxide with a few small carbon (graphite) particles. By contrast, Auger mapping of the RoD_N1 tribofilm revealed a surprising feature: the track was uniformly covered by a smooth metallic copper layer that could not have resulted from simple smearing of copper NPs under contact pressure and shear. The complete absence of oxygen or other elements indicates this layer consists of pure copper i.e. Cu (0). This suggests that the copper oxides detected by Raman spectroscopy on the tribofilm surface likely formed through oxidation of Cu (0) after the specimens were removed from the hydrogen atmosphere of the RCF testing chamber and exposed to air.

The Auger maps further show that the copper layer was sparsely covered by other materials. A large streak of material on the left side of the mapping image appears strongly in the iron and carbon maps, but weakly in the oxygen map, indicating that it is composed of iron oleate. Previous studies have shown that iron (II) oleate and Cu (0) are produced via the redox reaction between wear-generated nascent steel surfaces (Fe (0)) and 0.1 wt.% copper (II) oleate, catalysed by 0.05 wt.% free oleic acid in SN100 mineral oil, as described in **Eq. (1)** [14].

Cu^{2+} Oleate + $Fe^{0} \leftrightarrow Cu^{0}$ + Fe^{2+} Oleate **Eq. (1)**

Fe (0) can displace less electronegative metals from their oleate salts to form Fe (II) oleate and the corresponding metal (Me (0)), but four conditions are required to enable this redox reaction in oil: 1) the metal oleate must be soluble in the base oil (e.g. 0.1 wt.% metal oleate in base oil), 2) free oleic acid must be present in the lubricant to catalyse the redox reaction (e.g. 0.05 wt.% oleic acid in base oil), 3) the tribological conditions can involve either pure rolling or sliding, but require mixed/boundary lubrication, where thin-film rubbing exposes nascent iron surfaces, and 4) higher testing temperatures enhances reactivity and promote tribofilm formation e.g. a testing temperature of 100 °C produces thicker tribofilms than 40 °C [14], [23].

The tribological conditions in the present study fulfil all four of the previously discussed requirements, thereby allowing the redox reaction described by **Eq. (1)** to occur. RCF testing was performed under boundary lubrication, with pure rolling in the ball bearing (BoD) setup and a small degree of sliding (<10% SRR) at the roller edges in the RoD setup. Nanol™ contains copper NPs functionalized with copper oleate, as well as free oleic acid, and has good solubility in PAO oil. Finally, the testing temperature of 120 °C promoted the redox reaction and the generation of the tribofilm.

Raman and Auger analysis of the tribofilm have confirmed that the redox reaction (**Eq. (1)**) occurred on the wear track during RCF testing. The reaction kinetics are influenced by the operating conditions of the tribological contact e.g. sliding accelerates tribofilm formation.

Both, the previous study using copper oleate in air [14] and the present work with Nanol™ in hydrogen demonstrate that the same redox reaction, producing a copper tribofilm and iron oleate is responsible for low friction observed in both environments. Therefore, it can be concluded that the CoF will also remain low in a hydrogen environment.

When dispersed in low polarity PAO oil, Nanol™ reacted with the wear track to generate a tribofilm that substantially reduced friction. Similarly, commercial copper oleate containing oleic acid formed

thick boundary films in low polarity SN100 mineral oil, but such films did not form in the polar diethyl adipate ester oil [14]. Therefore, comparable behaviour can be expected from Nanol™ when dispersed in mineral oils or esters oils.

Nanol™ NPs also have the ability to instantly reduce friction and wear through a mechanical action. The tiny size (PSD ~ 20 nm) of the copper colloids facilitates their movement through the narrow separations between the moving parts and the NPs reduce the contact area during mixed or boundary lubrication.

Thus, the Nanol™ additive can reduce friction and wear in tribological contacts through a combination of immediate mechanical action and continuous redox reaction.

Although Nanol™ extended the fatigue life compared to PAO, the tests failed due to similar damage. To investigate this behaviour, BoD fatigue tests lubricated with Nanol™ were conducted over defined durations (eg. 21, 51 and 152 hours), followed by Raman analysis of the wear tracks. As shown in **Fig. 19**, a thick, uniform tribofilm covered the wear track after 21 hours, but with continued testing up to 152 hours, the film became thinner and more porous, while a copper-rich wear debris accumulated outside the wear tracks. This suggests that after the initial 21 hours, the balance between tribofilm growth and wear was disrupted, with tribofilm wear overcoming formation, ultimately leading to test failure due to flaking on the wear track. The observed film thinning may be related to the depletion or oxidation of the free oleic acid available in the Nanol™ concentrate during high-temperature RCF testing, a hypothesis that warrants further investigation.

Rollers wear track subsurface analysis

Serial sectioning and subsequent analysis using optical and SEM/EDX of the roller subsurface revealed significant differences in damage between the PAO and Nanol™ lubricated RCF tests. The types of damage observed at four depths are summarised in **Table 5**.

One test (RoD_O1) failed due to high vibrations, showing no roller flaking or subsurface damage. Test RoD_N1 failed due to flaking on a roller but similarly exhibited no subsurface damage. Three of the PAO lubricated tests failed because of extensive, branched WECs and microstructural alterations, while one test (RoD_O5) failed due to large fatigue cracks at a depth of 0.5 mm (**Fig. 20**). In contrast, rollers from the Nanol™ lubricated tests predominantly exhibited microstructure alterations, with three showing a few fine WECs and small WEA (**Fig. 21**).

Table 5. Roller subsurface damage at four depths (0.5-2 mm) beneath the wear track

Test	0.5 mm	1 mm	1.5 mm	2 mm
RoD_O1	No damage	No damage	No damage	No damage
RoD_O2	No damage	No damage	No damage	Fatigue cracks
RoD_O3	Altered microstructure, extended WECs	Altered microstructure	Altered microstructure	No damage
RoD_O4	Altered microstructure	Altered microstructure, extended WECs	Altered microstructure WEC	No damage
RoD_O5	Altered microstructure, extended WECs all around wear track	WECs all around wear track subsurface, altered microstructure	WECs around wear track subsurface	No damage
RoD_N1	No damage	No damage	No damage	No damage
RoD_N2	Altered microstructure, small WECs	Altered microstructure, small WECs	Altered microstructure, small WECs	No damage
RoD_N3	WECs	Altered microstructure	Altered microstructure	No damage
RoD_N4	Altered microstructure	Altered microstructure	Altered microstructure, one small WEC	No damage
RoD_N5	Altered microstructure	Altered microstructure	No damage	No damage

The reduced subsurface damage observed in rollers lubricated with Nanol™ compared to those with PAO helps explain their longer fatigue life. Although no direct correlation was found between fatigue life, hydrogen concentration in the bearings at the end of testing, and wear track profiles, the extended RCF life of Nanol™ lubricated bearings can be attributed to the consistently lower CoF. Nanol™ reduces friction both by immediately decreasing the contact area between moving parts and by continuously forming chemical tribofilms with characteristics associated with low friction, such as smooth, soft, thick copper layers covered by lubricious, oil-insoluble iron oleate, which collectively enhance fatigue life. The average CoF of Nanol™, measured in air but under similar tribological conditions, was six times lower than that of PAO. Friction plays a critical role in RCF testing as it continuously generates heat within a confined space [35] and induces tribomutation, e.g. changes in the composition and microstructure of the surface

layer due to frictional contacts that can lead to plastic deformation, cracks, delamination, expansion/contraction [36], elevated CoF, increased wear rates [37] and WEC formation.

By lowering contact friction and the associated heat generation, both the components and the lubricant benefit. For example, thermal expansion of tribological parts and the resulting wear are minimised, tribomutation is reduced, and the drop in lubricant viscosity with the corresponding reduction in film thickness is avoided. Consequently, the immediate and sustained friction reduction under boundary lubrication can extend RCF life of bearings.

Conclusions

Nanol™ additized PAO oil enhances the RCF lives of bearings operating in a hydrogen environment compared with the base oil alone. In ball bearings (BoD) tests, Nanol™ significantly increased fatigue life, whereas in roller bearing (RoD) the improvement was limited, likely due to the grooved damage formed on the inner side of the disc wear track because of the rollers' negative sliding.

Although no direct correlation was observed between fatigue life, wear loss and hydrogen concentration in the bearings, the significant, immediate, and sustained friction reduction provided by Nanol™ contributed to the extended RCF life in hydrogen environment.

Nanol™'s mechanism of lubrication is based on the combined effect of its mechanical and chemical actions. Mechanically, the NPs can rapidly enter the smallest separations between moving surfaces in mixed or boundary lubrication regimes, reducing the real contact area. This is followed by a chemical mechanism driven by the redox reaction with nascent steel sites on wear tracks.

Raman and Auger analysis of tribofilms formed by PAO and Nanol™ showed clear compositional differences. Raman spectra indicated that PAO generated tribofilms are primarily iron oxide (as magnetite), whereas Nanol™ derived films contain both inorganic (copper oxide, magnetite, carbon) and organic compounds. Auger etching and mapping further confirmed earlier findings that Nanol™ generates a uniform, smooth copper (0) layer covered by an oil-insoluble Fe (II) oleate paste both formed through redox reactions between Nanol™ and freshly exposed steel.

The exceptional low friction and antiwear properties of this Nanol™ tribofilm reduced subsurface damage and extended the RCF life of bearings in hydrogen. These results, combined with Nanol™'s established performance as a stable, effective lubricant additive in conventional applications (engines, industrial, energy etc.) support its adoption for lubrication of hydrogen technology.

Acknowledgement

The authors thank Nanol Technologies Oy for providing the Nanol™ concentrate.

References

[1] Ciruna, J. A., and Szieleit, H. J., 1973, "The effect of hydrogen on the rolling contact fatigue life of AISI 52100 and 440C steel balls," *Wear*, 24(1), pp. 107–118. https://doi: 10.1016/0043-1648(73)90207-X.

[2] Uyama, H., Yamada, H., Hidaka, H., and Mitamura, N., 2011, "The Effects of Hydrogen on Microstructural Change and Surface Originated Flaking in Rolling Contact Fatigue," *Tribol. Online*, 6(2), pp. 123–132. https://doi: 10.2474/trol.6.123.

[3] Kohara, M., Kawamura, T., and Egami, M., 2006, "Study on Mechanism of Hydrogen Generation from Lubricants," *Tribol. Trans.*, 49(1), pp. 53–60. https://doi: 10.1080/05698190500486324.

[4] Lu, R., Nanao, H., Kobayashi, K., Kubo, T., and Mori, S., 2010, "Effect of Lubricant Additives on Tribochemical Decomposition of Hydrocarbon Oil on Nascent Steel Surfaces," *J. Japan Pet. Inst.*, 53(1), pp. 55–60. https://doi: 10.1627/jpi.53.55.

[5] Fujita, S., Mitamura, N., and Murakami, Y., 2005, "Research of New Factors Affecting Rolling Contact Fatigue Life," in *World Tribology Congress III, Vol. 2*, ASMEDC, pp. 73–74. https://doi: 10.1115/WTC2005-63400.

[6] Mizuhara, K., Taki, T., and Yamanaka, K., 1993, "Anomalous cracking of bearing balls under a liquid-butane environment," *Tribol. Int.*, vol. 26, no. 2, pp. 135–142. https://doi: 10.1016/0301-679X(93)90022-S.

[7] Kino, N., 2003, "The influence of hydrogen on rolling contact fatigue life and its improvement," *JSAE Rev.*, 24(3), pp. 289–294. https://doi: 10.1016/S0389-4304(03)00035-3.

[8] Ray, D., Vincent, L., Coquillet, B., Guirandenq, P., Chene, J., and Aucouturier, M., 1980, "Hydrogen embrittlement of a stainless ball bearing steel," *Wear*, 65(1), pp. 103–111. https://doi: 10.1016/0043-1648(80)90012-5.

[9] Niste, V. B., Tanaka, H., Ratoi, M., and Sugimura, J., 2015, "WS_2 nanoadditized lubricant for applications affected by hydrogen embrittlement," *RSC Adv.*, vol. 5(51), pp. 40678–40687. https://doi: 10.1039/C5RA03127C.

[10] Tanaka, H., Niste, V. B., Abe, Y., and Sugimura, J., 2017, "The Effect of Lubricant Additives on Hydrogen Permeation Under Rolling Contact," *Tribol. Lett.*, 65(3), p. 94. https://doi: 10.1007/s11249-017-0877-x.

[11] Ratoi, M., Tanaka, H., Mellor, B. G., and Sugimura, J., 2020, "Hydrocarbon Lubricants Can Control

Hydrogen Embrittlement," *Sci. Rep.*, 10(1), p. 1361. https://doi: 10.1038/s41598-020-58294-y.

[12] Tanaka, H., Ratoi, M., and Sugimura, J., 2021, "The role of synthetic oils in controlling hydrogen permeation of rolling/sliding contacts," *RSC Adv.*, 11(2), pp. 726–738. https://doi: 10.1039/D0RA00294A.

[13] Haxel, G. B., Hedrick, J. B., Orris, G. J., Stauffer, P. H., and Hendley, J. W., 2002, "Rare earth elements: critical resources for high technology," https://doi: 10.3133/fs08702.

[14] Ratoi, M., Bovington, C., and Spikes, H., 2003, "In Situ Study of Metal Oleate Friction Modifier Additives," *Tribol. Lett.*, 14 (1), pp. 33–40, https://doi: 10.1023/A:1021714231949.

[15] Smirnov, V. M., and Shalunov, E. P., 2020, "Antifriction powder bronzes with mechanically alloyed copper-based granules," *IOP Conf. Ser. Mater. Sci. Eng.*, 709(3), p. 033030. https://doi: 10.1088/1757-899X/709/3/033030.

[16] Nielesen, W.D Jn, "Metallurgy of Copper-Base Alloys.", Copper Development Association Inc., accessed Nov. 21, 2025. https://www.copper.org/resources/properties/703_5/

[17] Ghaednia, H., Jackson, R. L., and Khodadadi, J. M., 2015, "Experimental analysis of stable CuO nanoparticle enhanced lubricants," *J. Exp. Nanosci.*, 10(1), pp. 1–18. https://doi: 10.1080/17458080.2013.778424.

[18] Gondolini, A., Mercadelli, E., Zin, V., Barison, S., and Sanson, A., 2020, "Easy preparation method of stable copper-based nanoparticle suspensions in lubricant engine oil," *Lubr. Sci.*, 32(5), pp. 205–217. https://doi: 10.1002/ls.1496.

[19] Ali, M. K. A., Hou, X., and Abdelkareem, M. A. A., 2020, "Anti-wear properties evaluation of frictional sliding interfaces in automobile engines lubricated by copper/graphene nanolubricants," *Friction*, 8(5), pp. 905–916. https://doi: 10.1007/s40544-019-0308-0.

[20] Asnida, M., Hisham, S., Awang, N. W., Amirruddin, A. K., Noor, M. M., Kadirgama, K., Ramasamy, D., Najafi, G., and Tarlochan, F., 2018, "Copper (II) oxide nanoparticles as additve in engine oil to increase the durability of piston-liner contact," *Fuel*, 212, pp. 656–667. https://doi: 10.1016/j.fuel.2017.10.002.

[21] Abdel-Rehim, A. A., Akl, S., and Elsoudy, S., 2021, "Investigation of the Tribological Behavior of Mineral Lubricant Using Copper Oxide Nano Additives," *Lubricants*, 9(2), p. 16. https://doi: 10.3390/lubricants9020016.

[22] Muhammad, A. I., Mohd Yusof, N. F., and Ripin, Z. M., 2023, "The tribological performance analysis of palm olein-based grease lubricants containing copper nanoparticle additive," *Proc. Inst. Mech. Eng. Part*

J J. Eng. Tribol., 237(12), pp. 2162–2177. https://doi: 10.1177/13506501231190695.

[23] Ratoi, M., Anghel, V., Bovington, C., and Spikes, H., 2000, "Mechanisms of oiliness additives," *Tribol. Int.*, 33(3–4), pp. 241–247. https://doi: 10.1016/S0301-679X(00)00037-2.

[24] Molahalli, V., Sharma, A., Bijapur, K., Soman, G., Shetty, A., Sirichandana, B., Patel, B. G. M., Chattham, N. and Hegde, G., 2024, "Properties, Synthesis, and Characterization of Cu-Based Nanomaterials," Copper-Based Nanomaterials in Organic Transformations. Srivastava and Srivastava, eds., ASC Symposium Series, ASC Washington, DC, USA, pp. 1–33. https://doi: 10.1021/bk-2024-1466.ch001.

[25] Gupta, H. and Kumar, N., 2025, "Examination of Heat Transfer and Thermophysical Properties in Copper Nanoparticles," *Int. J. Adv. Multidiscip. Sci. Res.*, 8(3). https://doi: https://doi.org/10.31426/ijamsr.2025.8.3.8131.

[26] Kumar, A., Gupta, T., and Shukla, A., 2023, "Investigation of Thermal and Tribological Behaviour of Oil Dispersed Oleic Acid-Functionalized CuO Nano-Particles in Gear Oil Nano-Lubricants," *J. Nanofluids*, 12(2), pp. 372–387. https://doi: 10.1166/jon.2023.1922.

[27] Rudnick, L. R. and Bartz W. J., 2020, "Comparison of Syntehtic, Mineral oil, and Bio-Based Lubricant Fluids", Synthetics, mineral oils, and bio-based lubricants : chemistry and technology. L. R. Rudnick, ed., CRC Press, Taylor and Francis Group, Boca Raton, Florida, USA,

[28] Tanaka, H., Morofuji, T., Enami, K., Hashimoto, M., and Sugimura, J., 2013, "Effect of Environmental Gas on Surface Initiated Rolling Contact Fatigue," *Tribol. Online*, 8(1), pp. 90–96. https://doi: 10.2474/trol.8.90

[29] Tanaka, H., Hashimoto, M., Sugimura, J., and Yamamoto, Y., 2005, "Rolling Contact Fatigue of Bearing Steel in Hydrogen Environment," in *World Tribology Congress III, Vol. 1*, ASMEDC, pp. 155–156. https://doi: 10.1115/WTC2005-64037.

[30] Otsu, T., Tanaka, H., Ohnishi, K., and Sugimura, J., 2011, "Simple Experiment on Permeation of Hydrogen into Steel in Cyclic Contact," *Tribol. Online*, 6(7), pp. 311–316. https://doi: 10.2474/trol.6.311.

[31] López-Uruñuela, F. J., Fernández-Díaz, B., Pagano, F., López-Ortega, A., Pinedo, B., Bayón, R., and Aguirrebeitia, J., 2021, "Broad review of 'White Etching Crack' failure in wind turbine gearbox bearings: Main factors and experimental investigations," *Int. J. Fatigue*, 145, p. 106091. https://doi: 10.1016/j.ijfatigue.2020.106091.

[32] Gutiérrez Guzmán, F., Oezel, M., Jacobs, G., Burghardt, G., Broeckmann, C., and Janitzky, T., 2017,

"Reproduction of white etching cracks under rolling contact loading on thrust bearing and two-disc test rigs," *Wear*, 390–391, pp. 23–32. https://doi: 10.1016/j.wear.2017.06.020.

[33] Otero, V., Sanches, D., Montagner, C., Vilarigues, M., Carlyle, L., Lopes, J. A., and Melo, M. J., 2014, "Characterisation of metal carboxylates by Raman and infrared spectroscopy in works of art," *J. Raman Spectrosc.*, 45(11–12), pp. 1197–1206. https://doi: 10.1002/jrs.4520.

[34] Shen, T. D., Ge, W. Q., Wang, K. Y., Quan, M. X., Wang, J. T., Wei, W. D., and Koch, C. C., 1996, "Structural disorder and phase transformation in graphite produced by ball milling," *Nanostructured Mater.*, 7(4), pp. 393–399. https://doi: 10.1016/0965-9773(96)00010-4.

[35] Jakubek, B., Grochalski, K., Rukat, W., and Sokol, H., 2022, "Thermovision measurements of rolling bearings," *Measurement*, 189, p. 110512. https://doi: 10.1016/j.measurement.2021.110512.

[36] Kehrwald, B. and Klaus, P., 2014, "Tribomutation," Encyclopedia of Lubricants and Lubrication, T. Mang ed., Springer Berlin, Heidelberg, Germany, pp. 2155–2167. https://doi: 10.1007/978-3-642-22647-2_41.

[37] Zhang, Y., Liang, F., Lin, Y., Chen, X. and Zhu, Y., 2024, "Mitigating friction and wear by pre-designed or tribo-induced heterostructures: an overview," *Mater. Res. Lett.*, 12(8), pp. 535–550. https://doi: 10.1080/21663831.2024.2356282.

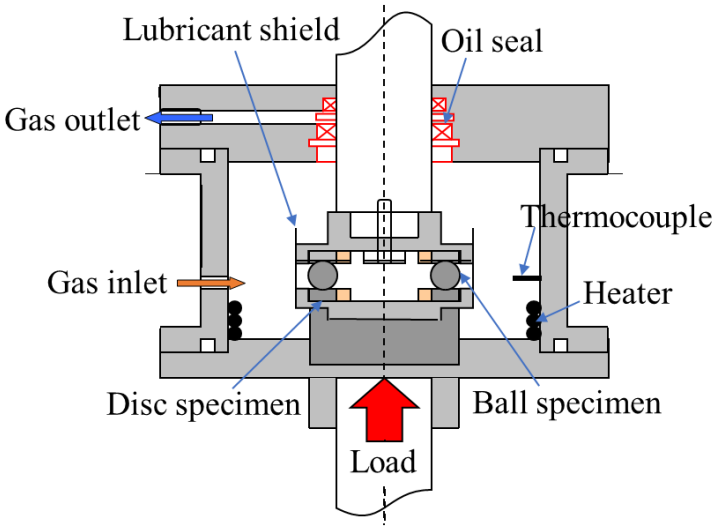

Fig. 1. RCF tribometer with ball-on-disc (BoD) setup

Fig. 2. Polymer cage of K81107T2 bearings with only three rollers positioned at 120° intervals, as used in the roller-on-disc setup

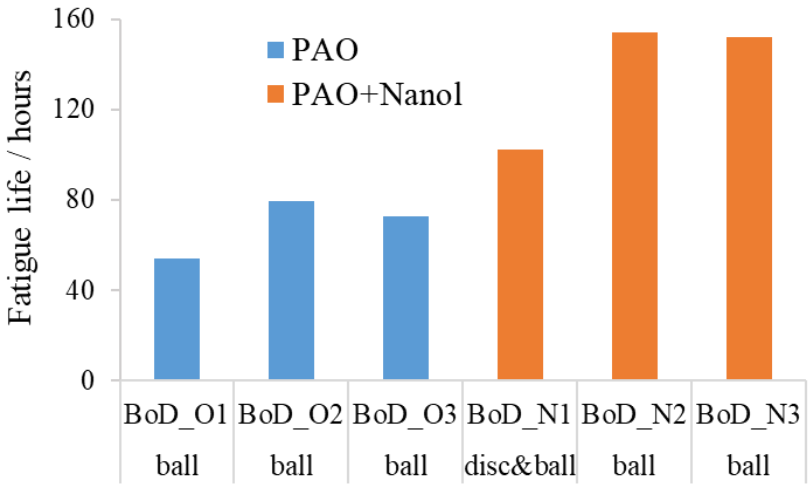

Fig. 3. Fatigue life of ball bearings (ball-on-disc setup) lubricated with PAO and PAO+Nanol^{TM}. All tests failed due to flaking on the balls, except for the BoD_N1 test, which exhibited flaking on both the disc and the ball

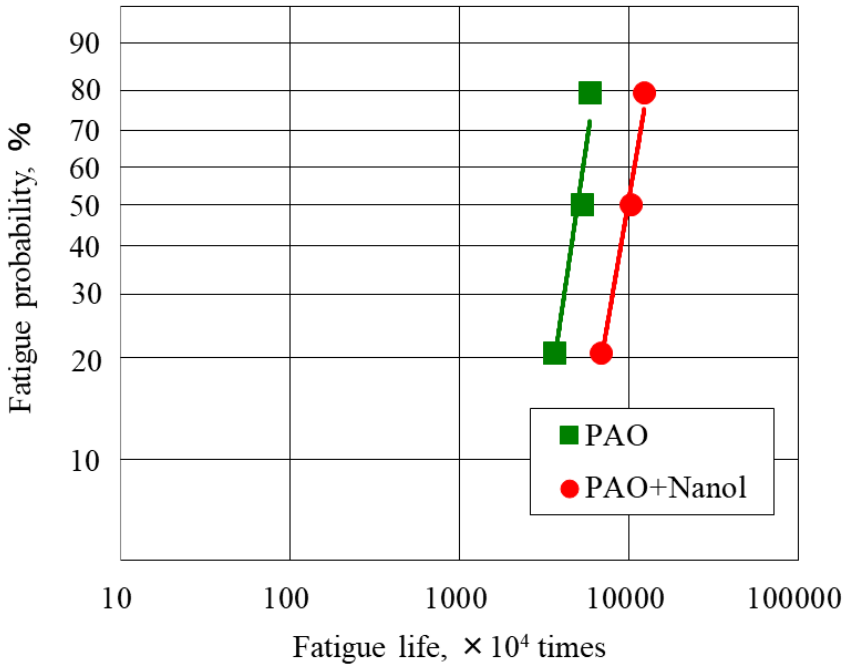

Fig. 4. Weibull plot comparing the fatigue lives of ball bearings (ball-on-disc setup) lubricated with PAO and PAO+Nanol™

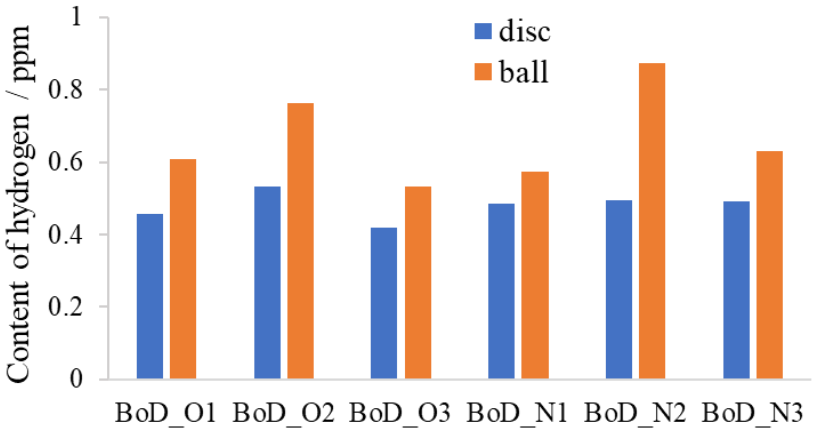

Fig. 5. Hydrogen content in disc and ball specimens from ball bearings (ball-on-disc setup) lubricated with PAO and PAO+Nanol™

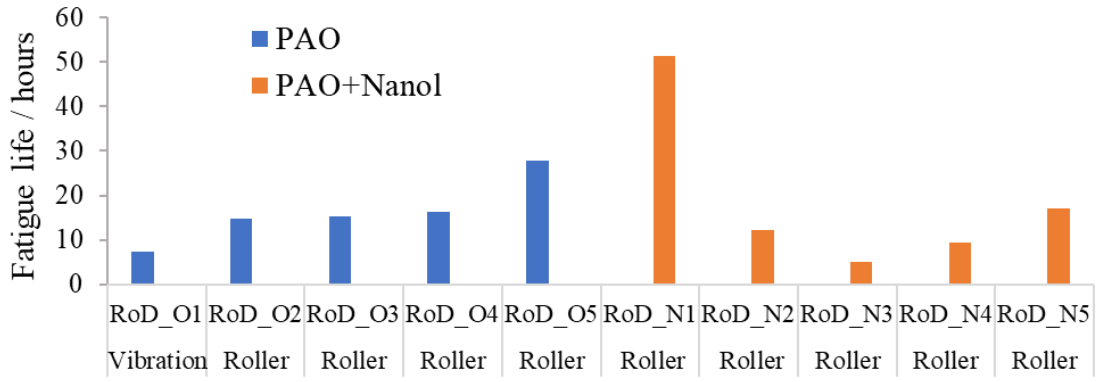

Fig. 6. Fatigue life of roller bearings (roller-on-disc setup) lubricated with PAO and PAO+Nanol™. All tests failed from flaking damage on the roller, except for the RoD_O1 test which was halted because of high vibration

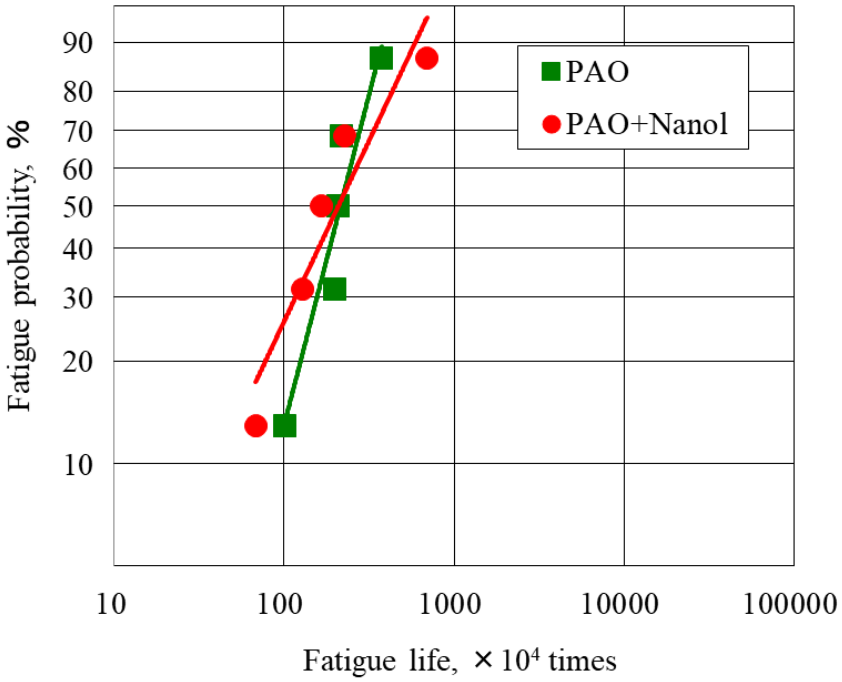

Fig. 7. Weibull plot comparing the fatigue lives of roller bearings (roller-on-disc setup) lubricated with PAO and PAO+Nanol™

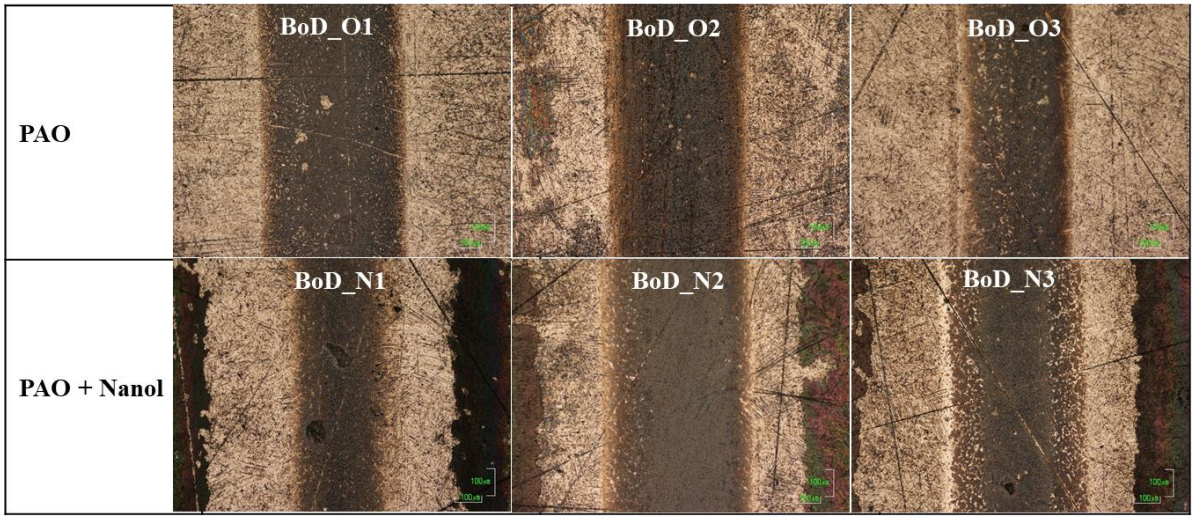

Fig. 8. Optical microscopy images of the disc wear track (100x magnification) from ball-on-disc tests lubricated with PAO and PAO+Nanol™. Scale bars represent 100 µm

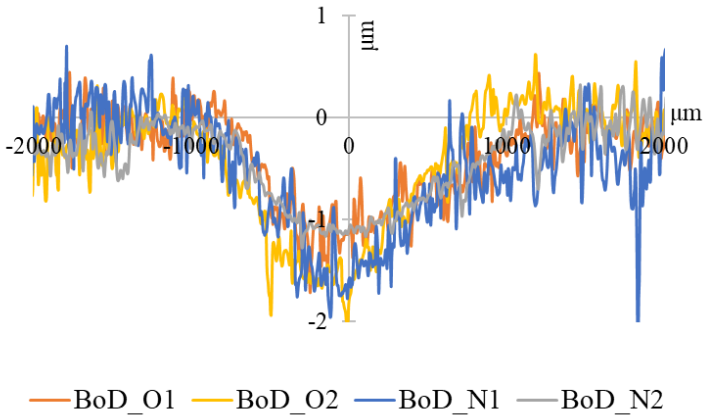

Fig. 9. Profilometry scans across disc wear tracks from ball-on-disc tests lubricated with PAO and PAO+Nanol™

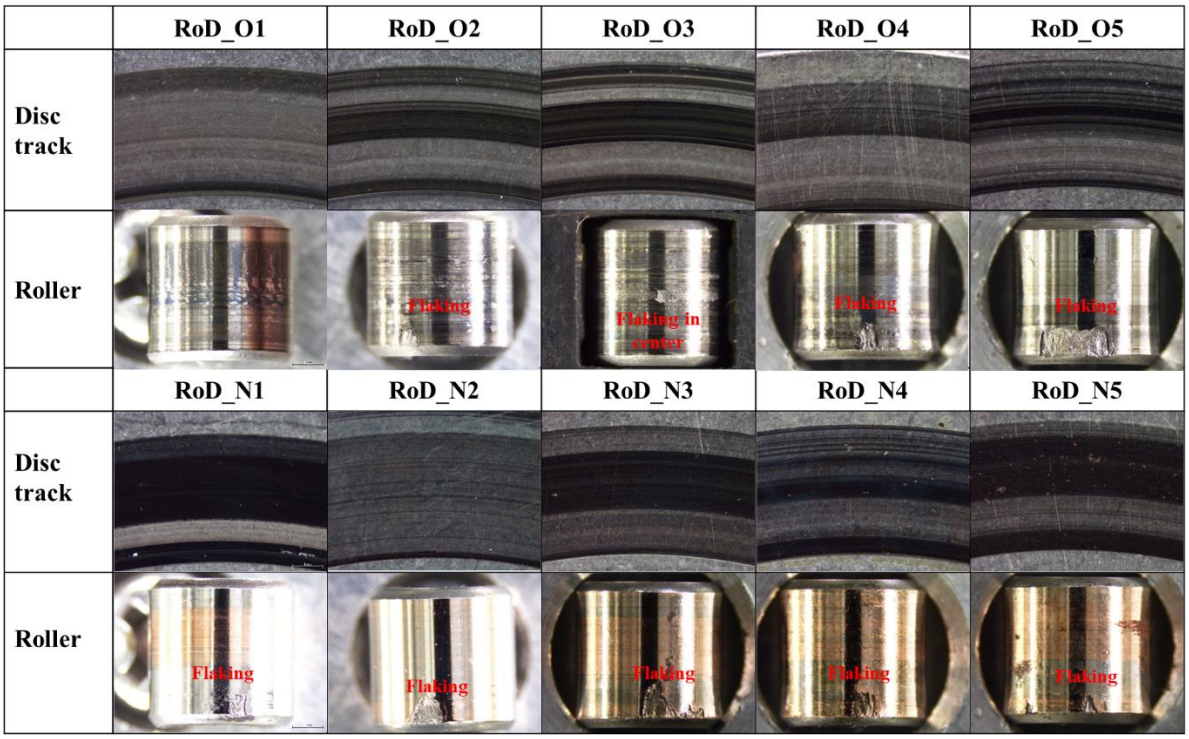

Fig. 10. Optical microscopy images (100x magnification) of the disc wear tracks and roller damage from roller-on-disc tests. On the rollers, the only observed damage was localized flaking, which in most cases occurred on the inner side of the rollers, except for RoD_O3 where it was located at the centre

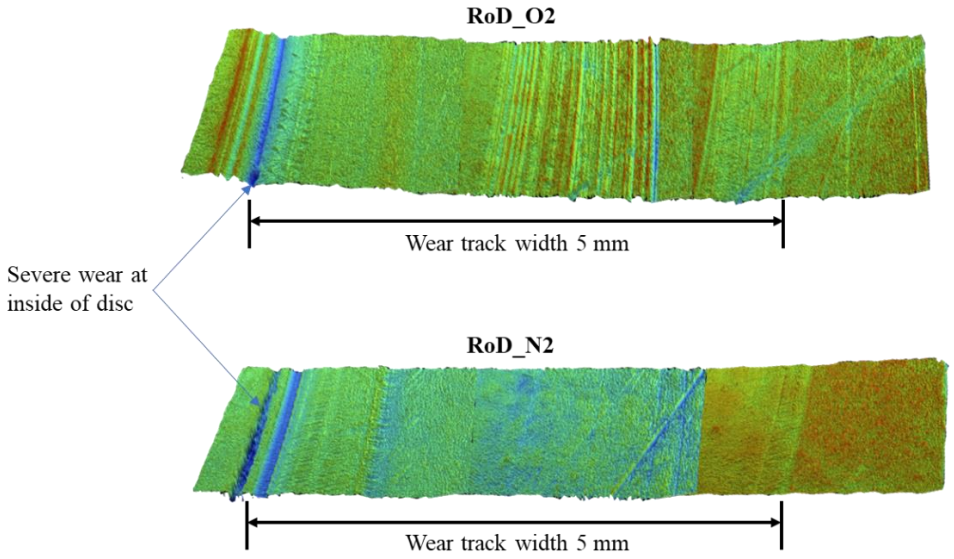

Fig. 11. Profilometry scans across disc wear tracks from roller-on-disc bearings lubricated with PAO and PAO+Nanol™

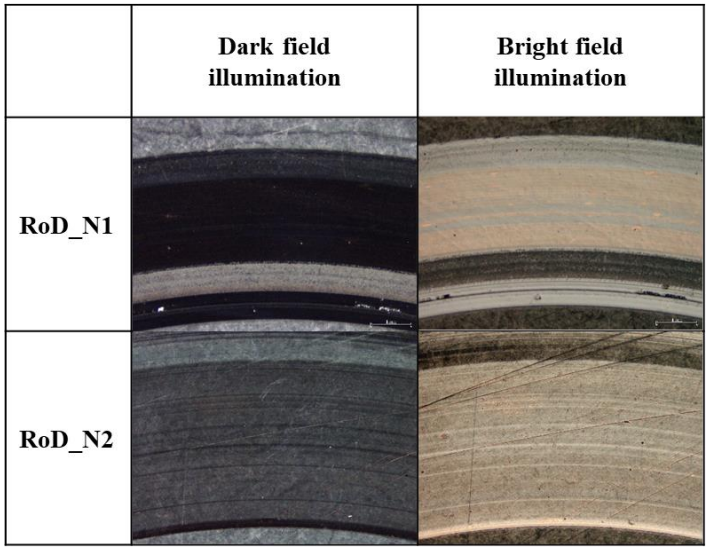

Fig. 12. Optical microscopy images (100x magnification) of PAO+Nanol^{TM} lubricated disc wear captured with dark field and bright field illumination. The bright field images illustrate the mirror like copper coating deposited on the disc wear tracks. Scale bars represent 1 mm

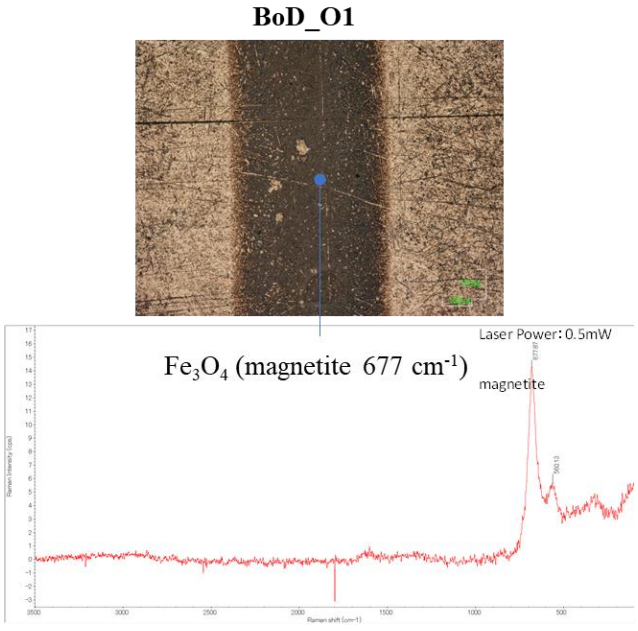

Fig. 13. Raman spectra of BoD_O1 acquired inside the disc wear track (100x magnification)

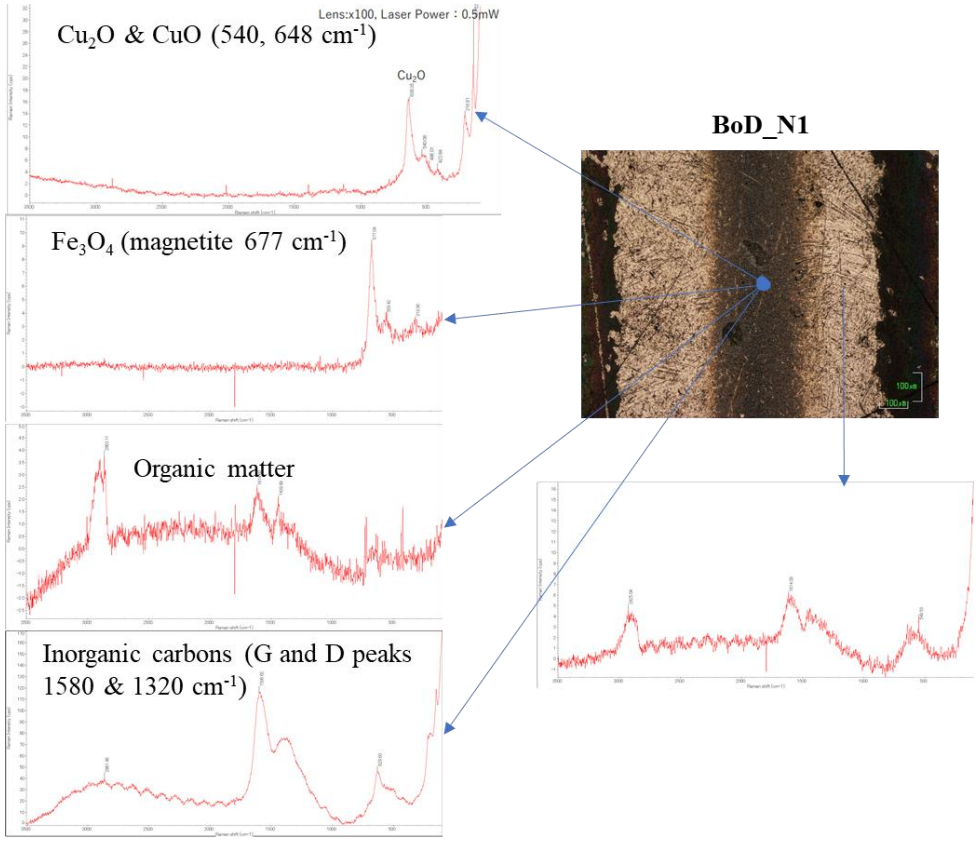

Fig. 14. Raman spectra of BoD_N1 acquired inside the disc wear track (100x magnification)

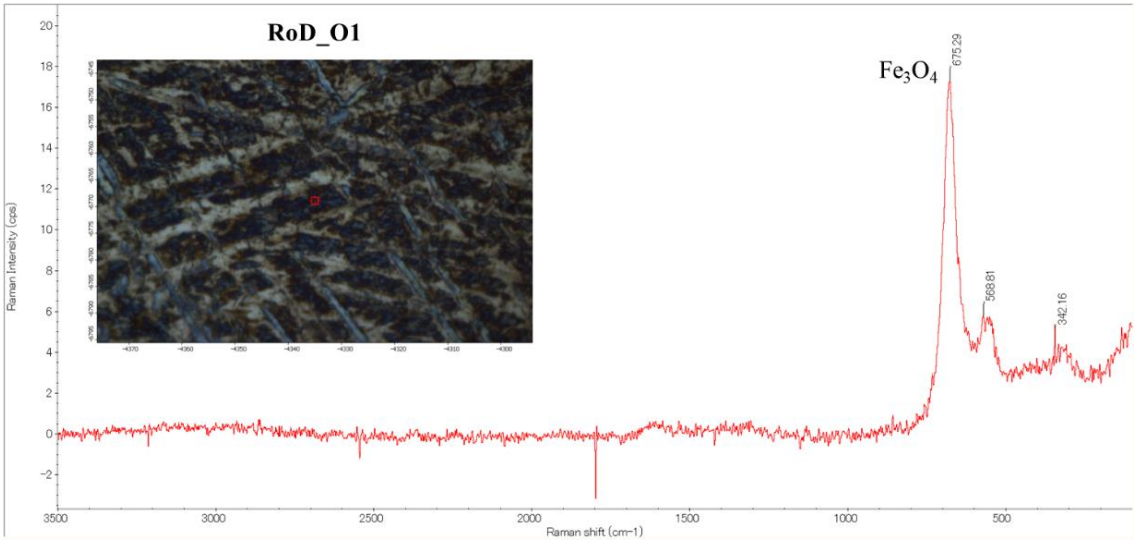

Fig. 15. Raman spectra of RoD_O1 acquired inside the disc wear track (100x magnification)

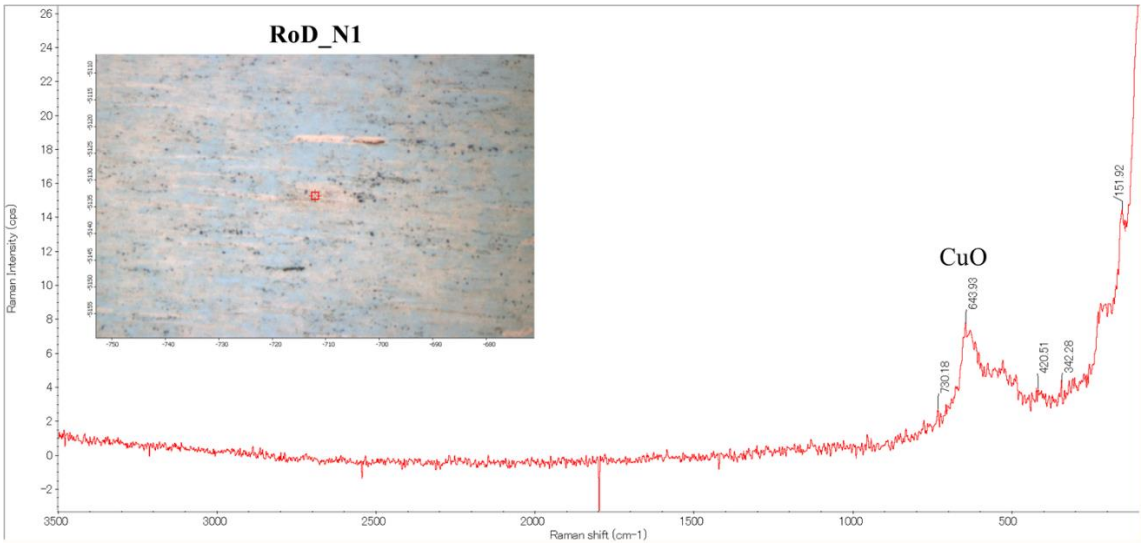

Fig. 16. Raman spectra of RoD_N1 acquired inside the disc wear track (100x magnification)

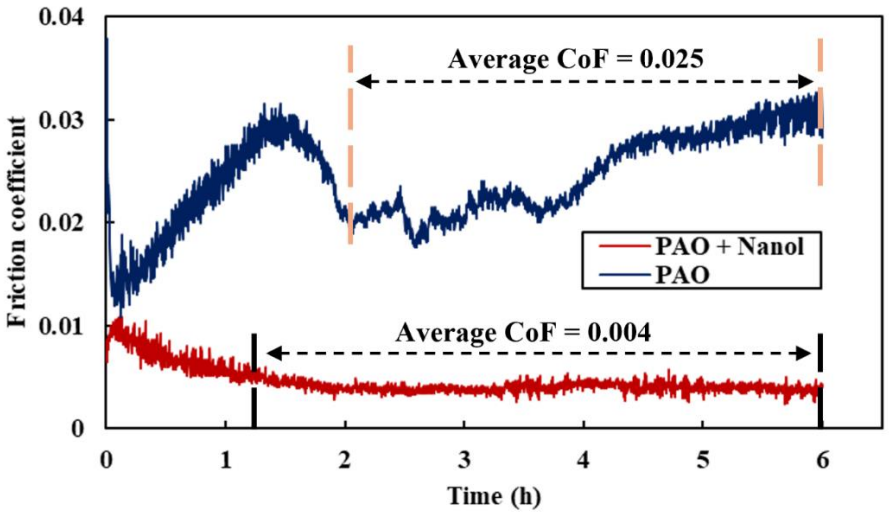

Fig. 17. Coefficient of friction for PAO and PAO+Nanol^{TM} obtained from MTM ball-on-disc tests

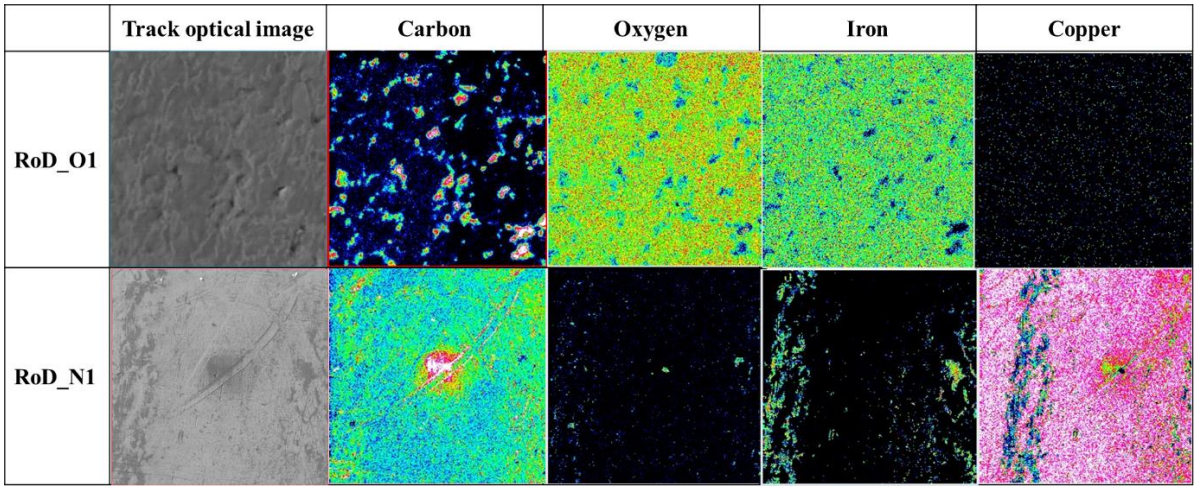

Fig. 18. Auger optical images and elemental maps of RoD_O1 and RoD_N1 taken inside the disc wear track after etching. Magnification x10000 (RoD_O1) and x1000 (RoD_N1)

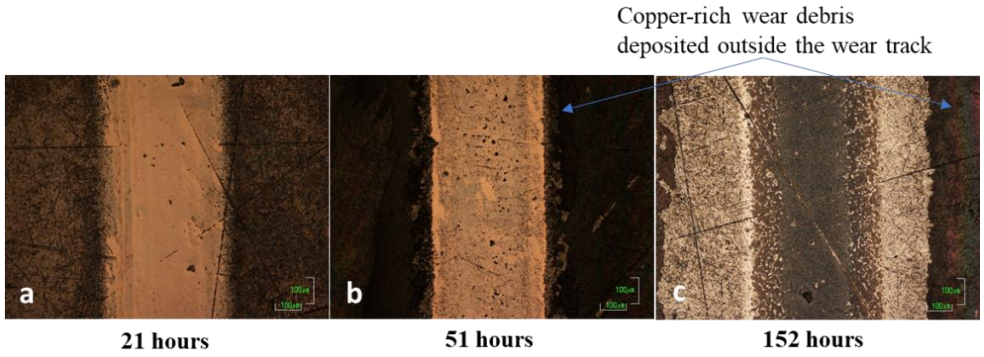

Fig. 19. Optical microscopy images of the disc wear track (100x magnification) from ball-on-disc tests lubricated with PAO+Nanol^{TM} after defined testing durations: (a) 21 hours, the track is covered by thick, uniform copper films, (b) 51 hours, the copper films became thinner, and (c) 152 hours, the test was halted due to flaking failure, and the copper films were observed to be even thinner. Scale bars in (**a-c**) represent 100 μm

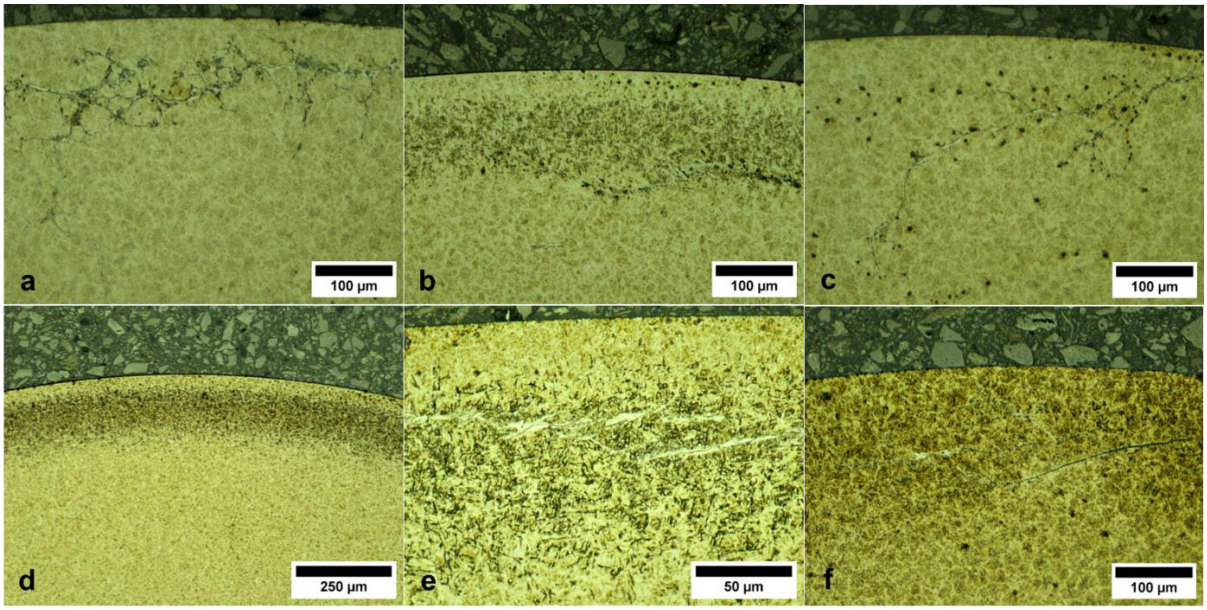

Fig. 20. Optical microscopy images showing subsurface damage in the roller wear track (a) WEC in RoD_O5 at 1 mm depth; (b) WECs and microstructure alteration in RoD_O5 at 0.5 mm depth; (c) WECs in RoD_O4 at 1 mm depth, (d) Microstructure alteration in RoD_N4 at 0.5 mm depth; (e) WECs and microstructure alteration in RoD_N2 at 0.5 mm depth; (f) WECs and fatigue cracks in RoD_N4 at 1.5 mm depth. Scale bars in (**a-c, f**) represent 100 µm, (**d**) 250 µm, and (**e**) 50 µm

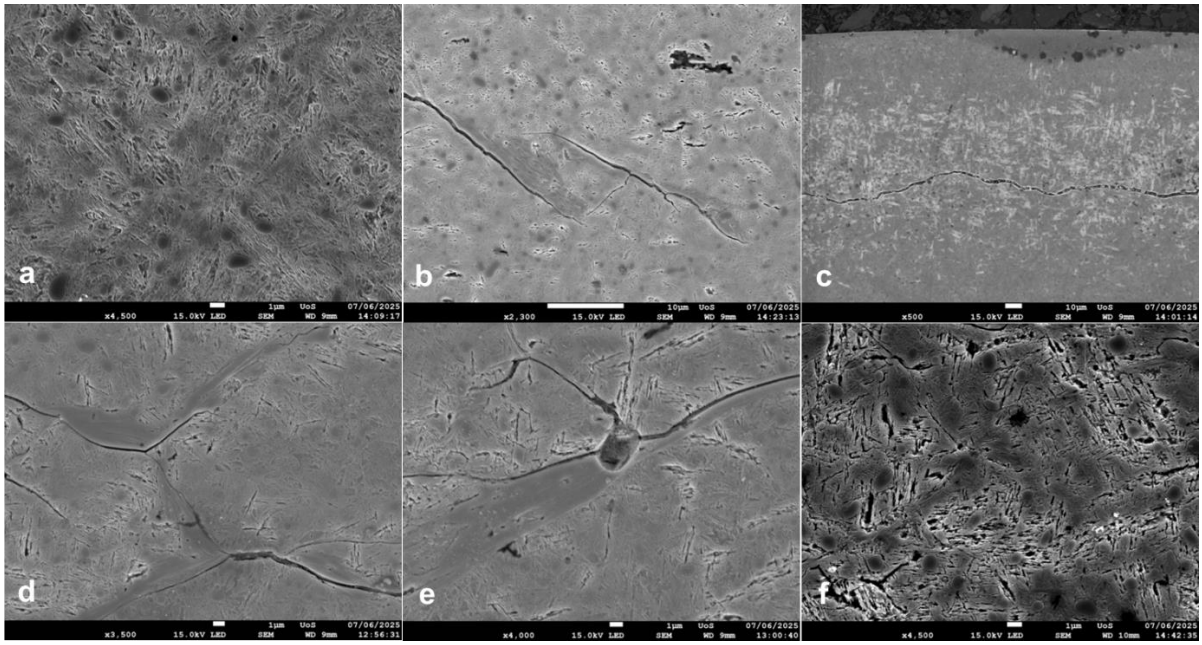

Fig. 21. SEM images of subsurface damage in the roller wear track at 0.5 mm depth: (a) Normal microstructure in RoD_O2; (b) WEC and inclusions in RoD_O3; (c) Fatigue crack and microstructure alteration in RoD_O5; (d) WEC and microstructure alterations RoD_O5; (e) WEC, microstructure alteration, and inclusion RoD_O5; (f) Microstructure alteration in RoD_N2. Scale bars in (**a-f**) represent 1 µm